

Diffuse-interface modeling of multiphase, multicomponent flows with phase change in the nondilute limit: application to melting and devolatilization of plastics

By D. Long[†], A. Mukherjee[†], S. Salimi[†], L. Brown, H. Collis, S. Mirjalili, S. S. Jain[‡], L. Brandt[¶] AND C. Schulze-Netzer[†]

This study explores the viability of diffuse-interface methods for simulating the plastic recycling process. Through an exploratory analysis of the relevant physics, we found promising results that support the use of the diffuse-interface method as a suitable modeling approach. We propose a multicomponent model for nondilute systems. Using simplified parameters, we achieved qualitatively reasonable results, including successful phase-change initiation and chemical species confinement to their respective phases, essential for accurate chemistry calculations during plastic recycling. While the methodology's algorithmic simplicity is an advantage, limitations include the need for finer grids and approximations of solid behavior through fluid-like modifications. Future work will refine the model, incorporate gas-phase chemistry, and potentially address solid deformation for more accurate simulations.

1. Introduction

Thermochemical recycling of plastics has gained much attention as a new possible solution to valorize currently unrecyclable polymer mixtures. We are particularly interested in the gasification process, as it promises to valorize multipolymer films and composites (Schulze-Netzer 2024). During gasification, plastic waste is treated with heat, resulting in melting and devolatilization or vaporization. The liquid and gaseous polymer mixtures also undergo chemical reactions, but solving for these chemical reactions in a computationally feasible manner is a separate challenge that we leave for future work.

In this study, we investigate the feasibility of using the diffuse-interface method to represent this gasification process appropriately. We approach this investigation by increasing the level of complexity of our multiphysics model sequentially. The first requirement is the representation of an arbitrary number of immiscible phases, which we denote with the term N phase and discuss in Section 2. Second, we construct each phase from an arbitrary number of confined chemical species. We call these M components and address these in Section 3. Finally, we add phase change from solid to liquid to our model and present this process in Section 4.

While multiphase flow models have been used for many years, the choice of model is not generally agreed upon. Boettinger *et al.* (2002) discuss a systematic way to derive

[†] Department of Energy and Process Engineering, Norwegian University of Science and Technology, Norway

[‡] George W. Woodruff School of Mechanical Engineering, Georgia Institute of Technology

[¶] Department of Environment, Land and Infrastructure Engineering, Politecnico di Torino, Italy

diffuse-interface models for solidification, which they accordingly call phase-field, based on a thermodynamic treatment. This framework has the advantage of being rooted in thermodynamics, whose laws should be satisfied for the highest level of confidence in simulation results, but has the disadvantage of requiring fourth-order derivatives in the transport equation for conserved quantities. Furthermore, the thermodynamic treatment requires prescribing an interpolation function, for which there are common choices but no clear physical reason to choose one function over any other. In contrast, second-order phase-field models were developed starting from the conservative diffuse-interface model of Chiu & Lin (2011), the conservative Allen-Cahn model of Brassel & Bretin (2011), and the accurate conservative diffuse-interface model of Jain (2022) through geometric arguments. One loses the firm grounding in thermodynamics, but requires only second derivatives and acquires desirable numerical properties such as maintaining positivity, boundedness, and conservation with an appropriate discretization (Mirjalili *et al.* 2020; Jain *et al.* 2020; Mirjalili & Mani 2021; Jain & Moin 2022). In order to facilitate multiphysics simulations of two-phase flows, Jain & Mani (2023) presented a model for scalar transport in two-phase flows that was later extended to heat and mass transfer across interfaces by Mirjalili *et al.* (2022). Subsequently, Mirjalili *et al.* (2022) presented consistent models for heat and mass transport.

We decided to utilize the conservative diffuse-interface family of models since an extension from two to N phase that has these desirable numerical properties was recently introduced by Mirjalili & Mani (2024). One could also start from the model developed by Huang *et al.* (2021), but their results use an implicit time-stepping scheme, which requires additional software infrastructure in order to efficiently precondition and solve the resulting linear system at each time step. This effort may be worthwhile in the future, but for our study the explicit time-stepping methods often used for conservative diffuse-interface models are desirable.

2. N phase flow

Diffuse-interface methods implicitly capture phase interfaces by solving transport equations for the volume fractions of different phases within the domain (Anderson *et al.* 1998; Mirjalili *et al.* 2017). These volume fractions are continuous functions and, hence, smear the interface between phases across a handful of computational cells. This modeling decision has the downside of relaxing the sharp interface between immiscible phases, yet it avoids explicitly tracking an interface. This is beneficial since interface tracking algorithms add computational expense, while with diffuse-interface methods, interfacial regions naturally arise from simply solving the partial differential equations.

We use the model developed by Mirjalili & Mani (2024) for N -phase flow, which is given by

$$\frac{\partial \phi_p}{\partial t} + \nabla \cdot (\mathbf{u} \phi_p) = \nabla \cdot \mathcal{R}_p, \quad (2.1)$$

where ϕ_p is the volume fraction of phase p , the regularization term is given by

$$\mathcal{R}_p = \Gamma \left(\varepsilon \nabla \phi_p - \sum_{q \neq p} \phi_p \phi_q \frac{\nabla \phi_{pq}}{|\nabla \phi_{pq}|} \right), \quad (2.2)$$

Γ is a parameter controlling the strength of the regularization force that separates phases,

ε is a parameter controlling the width of the interface, and

$$\phi_{pq} = \frac{\phi_p}{\phi_p + \phi_q}. \quad (2.3)$$

For all cases in this study, we choose $\Gamma(t) = \max(\mathbf{u}(t))$ and $\varepsilon = \Delta x = \Delta y$.

From Mirjalili & Mani (2024), we also have the Navier-Stokes equations

$$\frac{\partial \rho \mathbf{u}}{\partial t} + \nabla \cdot ((\rho \mathbf{u} - \mathcal{S}) \otimes \mathbf{u}) = -\nabla P + \nabla \cdot (\mu [\nabla \mathbf{u} + \nabla \mathbf{u}^\top]) + \rho \mathbf{g} + \mathcal{F}_{\text{ST}}, \quad (2.4)$$

$$\nabla \cdot \mathbf{u} = 0, \quad (2.5)$$

where

$$\mathcal{S} = \sum_p \rho_p \mathcal{R}_p, \quad (2.6)$$

is a correction to the Navier-Stokes to be consistent with the diffuse-interface method and the surface tension is given by

$$\mathcal{F}_{\text{ST}} = - \sum_{p < q} 6\sigma_{pq} \phi_p \phi_q \nabla \cdot \left(\frac{\nabla \phi_{pq}}{|\nabla \phi_{pq}|} \right) \nabla \phi_{pq} \quad (2.7)$$

where σ_{pq} is the surface tension coefficient between phases p and q .

Physical properties such as the density ρ and the viscosity μ are computed by averaging over the phases. For example,

$$\mu = \sum_p \phi_p \mu_p. \quad (2.8)$$

Using the model defined in Eqs. (2.1) and (2.4), we simulate a bubble rising through two fluids of differing densities, as shown in Figure 1. The domain is 0.024 m \times 0.048 m with 128 cells in the horizontal direction and 256 in the vertical direction. The transition between the two background fluids (orange and green in Figure 1) occurs at a height of 0.015 m. The bubble has a radius of 0.003 m, is centered horizontally, and is at a height of 0.006 m. We use this general geometry in all the simulations within this work. All initialized droplets or other circular shapes have a radius of 0.003 m, the transition between the background phases occurs at the same height, but the location of initialized droplets varies depending on the test we carry out.

When the bubble rises through ϕ_2 due to buoyancy, the surface tension pulls ϕ_2 upward (Figure 1(b,c)) until the bubble fully escapes. Then, ϕ_2 begins to descend due to gravity. This defines our base case, to which we now add further complexity. In the next step, we consider each phase to consist of many components. The overall behavior remains unchanged in comparison to Figure 1, but we include additional dynamics within each phase. Therefore, in the next section, we provide the model for M species and perform simulations to analyze the effect of adding it to the model.

3. M confined components

Let $Y_{p,c}$ be the mass fraction of component c in phase p . These mass fractions are defined such that

$$\sum_c Y_{p,c} = 1 \quad \forall p. \quad (3.1)$$

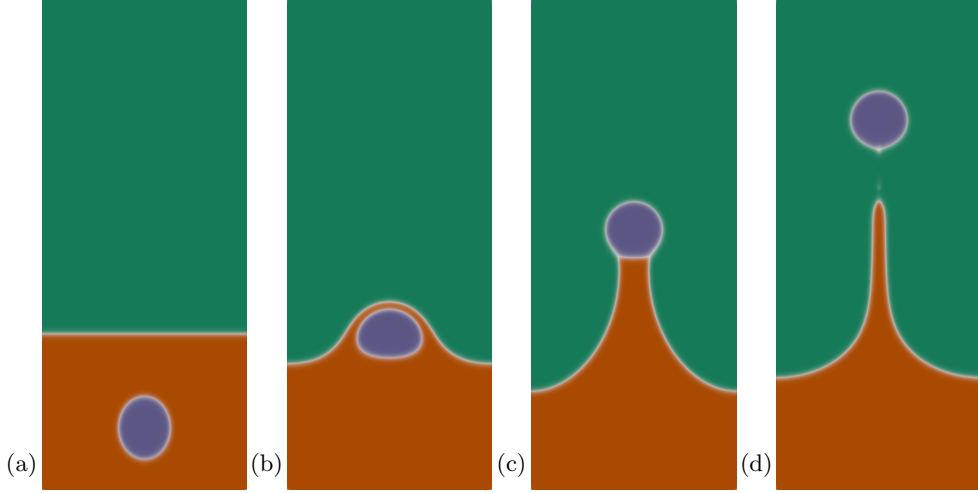


FIGURE 1. A low-density bubble (purple, ϕ_3) rising through two fluids of higher (orange, ϕ_2) and lower (green, ϕ_1) densities. The snapshots are taken at times (a) 0 s, (b) 0.1 s, (c) 0.2 s, and (d) 0.3 s. We use the physical constants $\rho_1 = 1000$, $\rho_2 = 1200$, $\rho_3 = 1$, $\mu_1 = 0.1$, $\mu_2 = 0.15$, $\mu_3 = 1 \times 10^{-4}$, $\sigma_{12} = 0.05$, and $\sigma_{13} = \sigma_{23} = 0.07$, following Mirjalili & Mani (2024).

Therefore, the appropriate mixture quantities to be transported are $\phi_p Y_{p,c}$. Using the consistent scalar transport formulation of Mirjalili *et al.* (2022), we find the transport equations for the chemical species to be

$$\frac{\partial \phi_p Y_{p,c}}{\partial t} + \nabla \cdot (\phi_p Y_{p,c} \mathbf{u}) = \nabla \cdot \left(\phi_p \mathcal{D}_{p,c} \frac{W_c}{\bar{W}_p} \nabla X_{p,c} \right) + \nabla \cdot (\mathcal{R}_p Y_{p,c}), \quad (3.2)$$

where $\mathcal{D}_{p,c}$ is the diffusion coefficient, W_c is the molecular weight of component c , \bar{W}_p is the mixture-averaged molecular weight of phase p , and $X_{p,c}$ is the molar fraction of component c within phase p . The diffusion coefficients can be computed through multi-component diffusion theory (Kee *et al.* 2017). Other diffusion models are also possible (e.g., see Coffee & Heimerl 1981) and can be formulated in the multiphase context in a straightforward way following the work of Mirjalili *et al.* (2022). The molecular weight of each phase is computed with the harmonic average

$$\bar{W}_p = \left(\sum_c \frac{Y_{p,c}}{W_c} \right)^{-1}, \quad (3.3)$$

and the molar fraction is given by

$$X_{p,c} = \frac{\bar{W}_p Y_{p,c}}{W_c}. \quad (3.4)$$

We aim to confine intraphase species masses to immiscible phases while remaining conservative during the diffusion process. Diffusion processes impose strict time-step limits when using realistic coefficients. Hence, we increase all species' diffusivity to $\mathcal{D}_{p,c} = 1 \times 10^{-3}$ for model testing.

Here, we would like to point out a numerical difficulty that needs to be addressed. Since we use the diffuse-interface approach, ϕ_p and $\phi_p Y_{p,c}$ are defined over the entire domain, including where they do not exist in reality. This results in two computations

that are prone to significant errors in floating point arithmetic

$$Y_{p,c} = \frac{\phi_p Y_{p,c}}{\phi_p}, \quad (3.5)$$

$$\phi_{p,q} = \frac{\phi_p}{\phi_p + \phi_q}. \quad (3.6)$$

As $\phi_p \rightarrow 0$, the value of $Y_{p,c}$ is ill-posed. Moreover,

$$\lim_{\phi_p, \phi_q \rightarrow 0} \frac{\phi_p}{\phi_p + \phi_q} \quad (3.7)$$

does not exist since the limit is path dependent. While Eq. (2.1) can circumvent this issue with a guarded division of the form

$$\phi_{p,q} = \frac{\delta + \phi_p}{\delta + \phi_p + \phi_q} \quad (3.8)$$

for a small value of δ , here $\delta = 1 \times 10^{-20}$, we found that Eq. (3.2) is not robust to this guarded division strategy. Our observation was that the ill-posedness of these quantities far from the interface caused spontaneous mass generation close to the spatial region where $\phi_p \approx \delta$. We adopt the following time-stepping strategy to avoid this issue:

- (a) Compute the updates $\phi_p^{(n+1)}$ and $(\phi_p Y_{p,c})^{(n+1)}$.
- (b) Clip $(\phi_p Y_{p,c})^{(n+1)}$ to remain between 0 and 1.
- (c) Consider $(\phi_p Y_{p,c})^{(n+1)}$ to accurately reflect only the relative species concentration.
- (d) Correct $(\phi_p Y_{p,c})^{(n+1)}$ by normalizing them such that their sum equals $\phi_p^{(n+1)}$.

Note that these numerical issues arise only far from the interface. Here, nonphysical values like negative concentrations have a more detrimental effect than disrupting theoretical convergence with ad hoc time-step corrections. We remark that this method is simplistic, and we hope future work or community contributions will offer a more elegant solution.

With these considerations in mind, we first test the conservation of the chemical species. Our goal is to verify that diffusion does not change the mass of each chemical species. We test this hypothesis with the static case presented in Figure 2. We set the gravitational constant to zero so that buoyancy does not induce any motion and initialize areas containing high concentrations of species 2 and 3 within phases ϕ_1 and ϕ_2 . Overall, ϕ_1 and ϕ_2 are composed of three spatially inhomogeneous components, as shown in Figure 2(a). The background is understood to be species 1, and we instantiate ϕ_3 with homogeneous concentrations; both are excluded from visualization.

Figure 2 shows the diffusive process where the concentrations of each species approach a uniform state over time. We observe the expected behavior as the concentration fields homogenize over time. For example, the uniform, steady-state concentration is reached at later times for regions where the initial concentration is particularly high or low compared to the steady-state profile.

Throughout the simulation we compute

$$\text{volume} = (\Delta x)^3 \sum_{\text{cells}} \phi_p Y_{p,c} \quad (3.9)$$

and expect this value to remain constant over time, up to rounding errors. We observe a maximum absolute deviation of 5.1×10^{-10} and a maximum relative deviation of 1.2%, which appears high, but we are considering small enough numbers that floating point arithmetic errors become dominant.

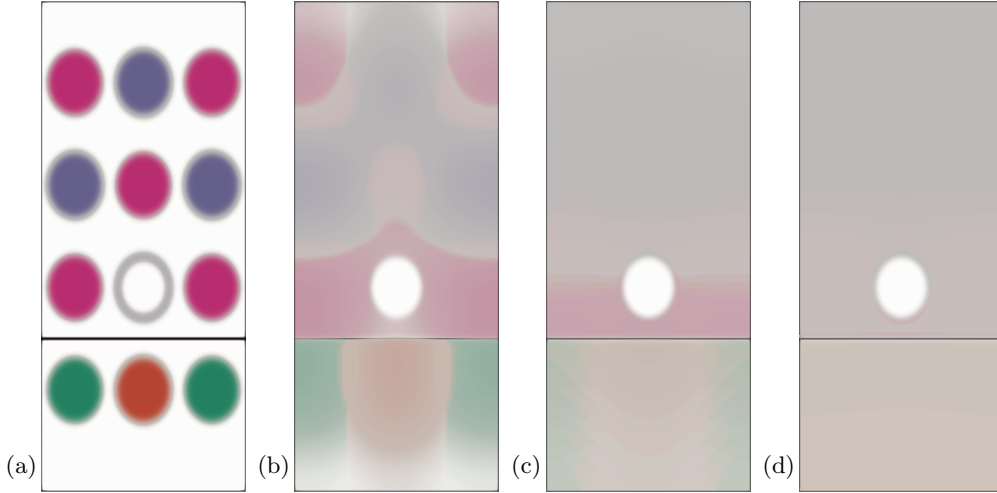


FIGURE 2. Static three-phase, three-component simulation showing diffusion of components within phases. The black horizontal line is the interface between the first and second phases. The white circle persisting through all four panels is the third phase. (a) The initial condition, where each color indicates an individual component. The first component of each phase is excluded from the visualization. (b) After 0.01 s, the local concentrations are still dominated by the initial configuration. (c) After 0.045 s, diffusion continues to drive the concentrations toward homogeneity. (d) After 0.09 s, the concentrations are essentially homogeneous throughout the domain.

Now, we reintroduce gravity and repeat the rising bubble case in Figure 1 and add an inhomogeneous initial concentration field. In each phase, $Y_{p,2}$ and $Y_{p,3}$ are set to 0.5 on the left boundary of their phase's domain and linearly decay to zero on the right boundary. $Y_{p,1}$ fills the rest of the space, decaying linearly from right to left starting with unity. In Figure 3, as expected, we see that the behavior of the phases is unaffected by the inhomogeneous initial concentration of the species. Within each phase, a roughly uniform concentration is reached by the time shown in Figure 3(b), which is a comparable time frame to the static case in Figure 2.

These two test cases serve as a preliminary validation of the coupling of N phases with M components under this diffuse-interface framework, as our current goal is to understand the feasibility of using the diffuse-interface method to simulate a recycling application. Therefore, in the following section, we consider one of the phases to be solid and describe an approach for modeling melting.

4. Phase change

In order to build toward the plastic gasification process, melting processes need to be modeled. Therefore, we modify our running model in Eqs. (2.1), (2.4), and (3.2) with processes occurring in a solid. Molecules within a solid are rigid, except when subjected to a large enough force, whereas fluids allow for more freedom in movement. The resulting first modification is simple: the diffusion coefficient within the solid is zero. The second modification is more complicated.

The solid needs to move as a unit. The traditional way to approach this requirement is to add a source term to the Navier-Stokes equations that encourages the velocity of the solid toward some specified value. This is typically done with a model reminiscent of

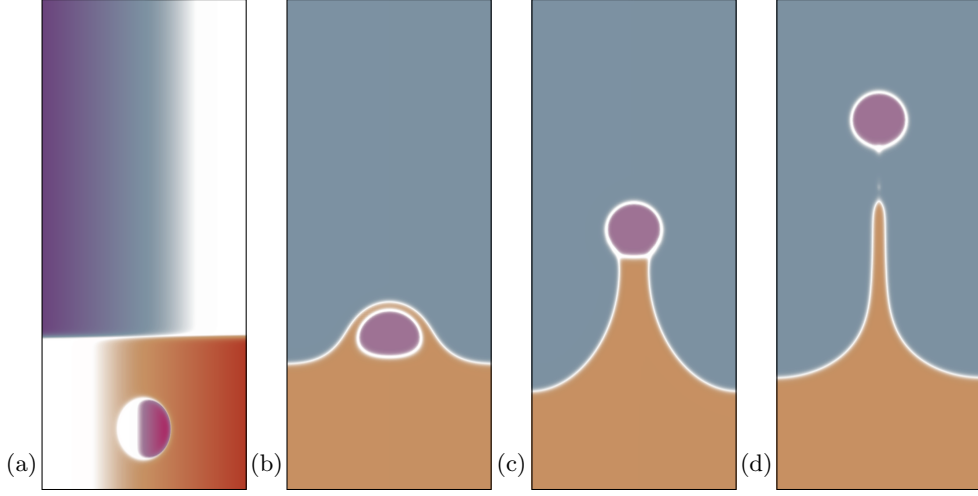


FIGURE 3. Repeating the bubble rise case in Figure 1 with phases composed of multiple chemical species. (a) The initial condition showing one species per phase. The concentration profile linearly decreases across the horizontal axis, where white space indicates an absence of that species. (b) After 0.1 s, concentrations have effectively reached a homogeneous state. (c) After 0.2 s. (d) After 0.3 s. The behavior of the phases is the same as with a single component, and the components remain confined within their respective phase.

Darcy's law in porous flow. That is, we add to Eq. (2.4) one of the terms

$$\mathcal{F}_{\text{rigid}} = \mathcal{C}\phi_S(\hat{\mathbf{u}} - \mathbf{u}) \quad \text{or} \quad \mathcal{F}_{\text{rigid}} = \mathcal{C}\frac{\phi_S^2}{(1 - \phi_S^3) + \epsilon}(\hat{\mathbf{u}} - \mathbf{u}), \quad (4.1)$$

where \mathcal{C} is a numerical parameter intended to overwhelm the viscous and gravitational forces in the Navier-Stokes equation, $\hat{\mathbf{u}}$ is the velocity the solid should take (assumed to be zero for simplicity), and ϵ is also a numerical parameter. We use the first model that is linear in ϕ_S following Hester *et al.* (2020), who describe an approach to estimate \mathcal{C} . The other model has been analyzed in the context of diffuse-interface methods by Huang *et al.* (2022), and performing a detailed comparison between the two penalization terms would be an interesting future analysis.

We also need a phase-change model that describes the solid melting into a liquid. We use the approach by Brown *et al.* (2023), wherein the following source term is added to the transport equation for the solid phase

$$\mathcal{S}_{\text{melt}} = \gamma\phi_S\phi_L(T_{\text{melt}} - T), \quad (4.2)$$

where γ is a parameter describing the melt rate, ϕ_L is the particular liquid that the solid becomes, T is the temperature, and T_{melt} is the melting temperature of the solid. This model can be derived as done by Brown *et al.* (2023) through a geometric argument, or through a thermodynamic argument as discussed by Boettinger *et al.* (2002).

The corresponding equation for ϕ_L has this source term subtracted from it, and the chemical species undergo phase change with the source term

$$\mathcal{S}_{\text{melt},c} = \gamma\phi_S\phi_L(T_{\text{melt}} - T)Y_{S,c}. \quad (4.3)$$

To understand the melting model qualitatively, we set $\gamma = 1$ and $T_{\text{melt}} - T = -100$. In a realistic scenario, the temperature would initially be below the melting temperature and increase due to an imposed heating rate by the gasification chamber. Mathematically,

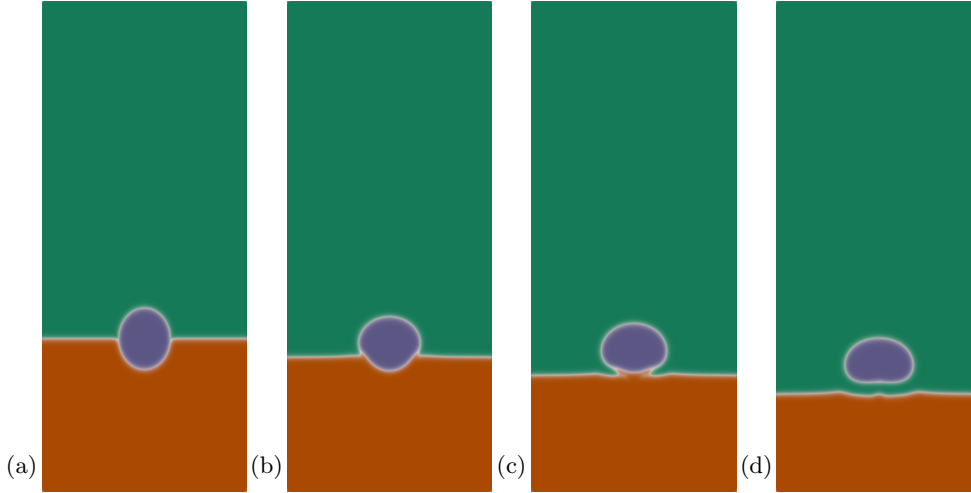


FIGURE 4. A case of a solid phase (orange) melting into a liquid phase (green) while a third phase (purple) coexists in the medium. (a) The initial condition where the droplet is held up by the solid. (b) Melting occurs only where orange contacts green. As such, some material is left underneath the droplet, and the droplet sags over this ledge due to surface tension. (c) As melting progresses, the droplet remains supported as the green liquid needs to flow in from the sides to initiate melting underneath. (d) The supportive solid is finally completely melted, and the droplet begins to descend while the solid continues melting.

this means that in the future we will couple our current methodology with an appropriate energy equation with boundary conditions that reflect operating conditions.

We add Eqs. (4.1)-(4.3) to the model and test the effect of melting, as depicted in Figure 4. We initialize the solid material, ϕ_S , on the bottom of the domain and the liquid it melts into, ϕ_L , on the top half. A third fluid, ϕ_F , is placed at the interface. As time passes, melting occurs only at the ϕ_S - ϕ_L interface. One can see this melting in Figure 4(b,c) where some solid persists underneath ϕ_F until ϕ_L fills in the area and contacts the solid. In Figure 4(d), the material holding up ϕ_F fully melts, and since $\rho_F > \rho_L$ in this circumstance, the remainder of the simulation proceeds with the solid gradually melting while the droplet descends.

While the results in Figure 4 align with how we expect the underlying partial differential equations to behave, whether we have captured enough of the solid's behavior to have a useful representation of the physical process is less clear. For example, we have a penalty term that encourages the solid velocity to be zero, but the partial differential equations do not strictly require it. We need to investigate the necessity of capturing these aspects of solid mechanics in subsequent analyses to keep the computational expense at a manageable level. Also unclear is how much deformation a plastic particle will experience or whether it will simply melt so rapidly that the deformation does not matter. Unfortunately, experimental data are limited when it comes to details such as these, so we will need to keep these questions, among others, in mind as we continue toward an application-ready numerical methodology.

5. Conclusions

In this study, we aimed to investigate whether diffuse-interface methods are a viable path toward simulating the plastic recycling process. We propose a multicomponent,

multiphase model in the limit of nondilute species along with phase-change effects. We performed an exploratory analysis of a subset of the necessary physics and found promising results that suggest the diffuse-interface method is a worthwhile modeling paradigm for our application. Using unphysical parameter values to facilitate more favorable and less expensive numerics, we have qualitatively reasonable results in coupling the various models we discussed. Notably, we are able to initiate phase change and confine chemical species to their appropriate phase. Both are key for the accurate chemistry calculations we will need to perform to understand the chemical species that are created in the recycling process.

No reactions occur in solid plastic, but once it melts, reactions happen in the liquid and gas phases. As we refine the model, we must ensure that the melting rate matches experimental data to confirm the timing of the chemistry. In a similar way, it is necessary to incorporate and verify the phase transition from liquid to gas (e.g., see Salimi *et al.* 2024).

A key advantage of the diffuse-interface method is its algorithmic simplicity. Many of the equations have a similar form, so efficient numerical algorithms can be developed more quickly as we move toward realistic scenarios because of the overlap between the equations. A disadvantage of this methodology is that it requires a finer grid than necessary when fixed grids are employed. However, this downside can likely be mitigated with adaptive mesh refinement (see, e.g., Loubère *et al.* 2023). Another disadvantage is that we approximate the behavior of a solid through modifications of the fluid momentum equation. Of course, we cannot replicate solid deformation without considering stresses and a more realistic simulation will require incorporating the stress tensor. However, the solid may melt so rapidly in realistic applications that the details of the solid deformation are negligible. Future studies in this area will be necessary.

Acknowledgments

The authors acknowledge the CTR summer program sponsors for the travel scholarship.

REFERENCES

- ANDERSON, D., MCFADDEN, G. & WHEELER, A. 1998 Diffuse-interface methods in fluid mechanics. *Annu. Rev. Fluid Mech.* **30**, 139–165.
- BOETTINGER, W. J., WARREN, J. A., BECKERMANN, C. & KARMA, A. 2002 Phase-field simulation of solidification. *Ann. Rev. Mater. Res.* **32**, 163–194.
- BRASSEL, M. & BRETIN, E. 2011 A modified phase field approximation for mean curvature flow with conservation of the volume. *Math. Methods Appl. Sci.* **10**, 1157–1180.
- BROWN, L., JAIN, S. & MOIN, P. 2024 A phase field model for simulating the freezing of supercooled liquid droplets. *SAE Int. J. Adv. & Curr. Prac. in Mobility* **6**, 1150–1157.
- CHIU, P.-H. & LIN, Y.-T. 2011 A conservative phase field method for solving incompressible two-phase flows. *J. Comput. Phys.* **230**, 185–204.
- COFFEE, T. & HEIMERL, J. 1981 Transport algorithms for premixed, laminar steady-state flames. *Combust. Flame* **43**, 273–289.
- HESTER, E. W., COUSTON, L.-A., FAVIER, B., BURNS, K. J. & VASIL, G. M. 2020 Improved phase-field models of melting and dissolution in multi-component flows. *P. R. Soc. A* **476**, 2020.0508.
- HUANG, Z., LIN, G. & ARDEKANI, A. M. 2021 A consistent and conservative model

- and its scheme for N -phase- M -component incompressible flows. *J. Comput. Phys.* **434**, 110229.
- HUANG, Z., LIN, G. & ARDEKANI, A. M. 2022 A consistent and conservative phase-field model for thermo-gas-liquid-solid flows including liquid-solid phase change. *J. Comput. Phys.* **449**, 110795.
- JAIN, S. S., MANI, A. & MOIN, P. 2020 A conservative diffuse-interface method for compressible two-phase flows. *J. Comput. Phys.* **418**, 109606.
- JAIN, S. S. & MOIN, P. 2022 A kinetic energy- and entropy-preserving scheme for compressible two-phase flows. *J. Comput. Phys.* **464**, 111307.
- JAIN, S. S. 2022 Accurate conservative phase-field method for simulation of two-phase flows. *J. Comput. Phys.* **469**, 111529.
- JAIN, S. S. & MANI, A. 2023 A computational model for transport of immiscible scalars in two-phase flows. *J. Comput. Phys.* **476**, 111843.
- KEE, R. J., COLTRIN, M. E., GLARBORG, P. & ZHU, H. 2017 *Chemically Reacting Flow: Theory, Modeling, and Simulation*. Wiley.
- LOUBÈRE, R., TURPAULT, R. & BOURRIAUD, A. 2023 A mood-like compact high order finite volume scheme with adaptive mesh refinement. *Appl. Math. Comput.* **443**, 127792.
- MIRJALILI, S., JAIN, S. S. & DODD, M. 2017 Interface-capturing methods for two-phase flows: an overview and recent developments. *Annual Research Briefs*, Center for Turbulence Research, Stanford University, pp. 117–135.
- MIRJALILI, S., IVEY, C. B. & MANI, A. 2020 A conservative diffuse interface method for two-phase flows with provable boundedness properties. *J. Comput. Phys.* **401**, 109006.
- MIRJALILI, S. & MANI, A. 2021 Consistent, energy-conserving momentum transport for simulations of two-phase flows using the phase field equations. *J. Comput. Phys.* **426**, 109918.
- MIRJALILI, S., JAIN, S. S. & MANI, A. 2022 A computational model for interfacial heat and mass transfer in two-phase flows using a phase field method. *Int. J. Heat Mass Tran.* **197**, 123326.
- MIRJALILI, S., KHANWALE, M., & MANI, A. 2022 Consistent modeling of scalar transport in multiphase flows using conservative phase field methods. *Annual Research Briefs*, Center for Turbulence Research, Stanford University, pp. 167–178.
- MIRJALILI, S. & MANI, A. 2024 A conservative second order phase field model for simulation of N -phase flows. *J. Comput. Phys.* **498**, 112657.
- SALIMI, S. Z., MUKHERJEE A., PELANTI M. & BRANDT L. 2024 A low Mach number diffuse-interface model for multicomponent two-phase flows with phase change. SSRN.
- SCHULZE-NETZER, C. 2024 Gasification for material recycling—a solution to the plastic flood? *Can. J. Chem. Eng.* **102**, 2966–2979.